AGU PUBLICATIONS

Geochemistry, Geophysics, Geosystems

RESEARCH ARTICLE
10.1002/2016GC006313

Geodetically constrained models of viscoelastic stress transfer and earthquake triggering along the North Anatolian fault

Phoebe M. R. DeVries[1], Plamen G. Krastev[2], and Brendan J. Meade[1]

[1]Department of Earth and Planetary Sciences, Harvard University, Cambridge, Massachusetts, USA, [2]Research Computing, Harvard University, Cambridge, Massachusetts, USA

Key Points:
- A geodetically constrained three-dimensional viscoelastic stress transfer model along the North Anatolian fault is developed
- Results suggest that viscoelastic stress transfer may play a major role in increasing stress at the locations of future earthquakes

Supporting Information:
- Supporting Information S1
- Figure S1
- Figure S2
- Figure S3
- Figure S4
- Figure S5
- Table A1

Correspondence to:
P. M. R. DeVries,
phoeberobinson@fas.harvard.edu

Citation:
DeVries, P. M. R., P. G. Krastev, and B. J. Meade (2016), Geodetically constrained models of viscoelastic stress transfer and earthquake triggering along the North Anatolian fault, *Geochem. Geophys. Geosyst.*, *17*, doi:10.1002/2016GC006313.

Received 23 FEB 2016
Accepted 14 JUN 2016
Accepted article online 20 JUN 2016

Abstract Over the past 80 years, 8 $M_W > 6.7$ strike-slip earthquakes west of 40° longitude have ruptured the North Anatolian fault (NAF) from east to west. The series began with the 1939 Erzincan earthquake in eastern Turkey, and the most recent 1999 $M_W = 7.4$ Izmit earthquake extended the pattern of ruptures into the Sea of Marmara in western Turkey. The mean time between seismic events in this westward progression is 8.5 ± 11 years (67% confidence interval), much greater than the timescale of seismic wave propagation (seconds to minutes). The delayed triggering of these earthquakes may be explained by the propagation of earthquake-generated diffusive viscoelastic fronts within the upper mantle that slowly increase the Coulomb failure stress change (ΔCFS) at adjacent hypocenters. Here we develop three-dimensional stress transfer models with an elastic upper crust coupled to a viscoelastic Burgers rheology mantle. Both the Maxwell ($\eta_M = 4 \times 10^{18} - 1 \times 10^{19}$ Pa s) and Kelvin ($\eta_K = 1 \times 10^{18} - 1 \times 10^{19}$ Pa s) viscosities are constrained by studies of geodetic observations before and after the 1999 Izmit earthquake. We combine this geodetically constrained rheological model with the observed sequence of large earthquakes since 1939 to calculate the time evolution of ΔCFS changes along the North Anatolian fault due to viscoelastic stress transfer. Apparent threshold values of mean ΔCFS at which the earthquakes in the eight decade sequence occur are between ~0.02 to ~3.15 MPa and may exceed the magnitude of static ΔCFS values by as much as 177%. By 2023, we infer that the mean time-dependent stress change along the northern NAF strand in the Marmara Sea near Istanbul, which may have previously ruptured in 1766, may reach the mean apparent time-dependent stress thresholds of the previous NAF earthquakes.

1. Introduction

Observations of pairs and sequences of large earthquakes, such as the 1992 $M_W = 7.3$ Landers and 1999 $M_W = 7.1$ Hector Mine earthquakes in the Eastern California Shear Zone and the 1939–1999 North Anatolian fault (NAF) earthquake sequence, suggest that stress changes in the crust due to one large earthquake may trigger subsequent earthquakes [e.g., *Pollitz and Sacks*, 2002; *Stein et al*., 1997]. The NAF has experienced a particularly remarkable sequence of eight large ($M_W > 6.7$) earthquakes since 1939 [*Barka*, 1996, 1999]. These earthquakes have ruptured the fault largely from east to west and have occurred at relatively regular intervals of 3–32 years. The coherent spatial and temporal patterns of these earthquakes represent an opportunity to understand how stress changes due to each earthquake may affect the next earthquakes in the sequence.

In recent decades, several stress transfer mechanisms have been invoked to explain patterns of both far-field and near-field triggered seismicity after earthquakes. Here we focus on previous studies that are directly relevant to this paper and leave more comprehensive discussions of earthquake triggering and stress transfer to review papers [*King et al*., 1994; *Harris*, 1998; *King and Cocco*, 2001; *Stein*, 2003; *Steacy et al*., 2005; *Freed*, 2005].

Static stress changes from large earthquakes (elastic stress changes due to fault slip only) have been used to explain continental earthquake sequences in New Zealand, California, Turkey and the northern Aegean, and many other tectonic settings worldwide [e.g., *Doser and Robinson*, 2002; *Parsons and Dreger*, 2000; *Verdecchia and Carena*, 2015; *Deng and Sykes*, 1997a, 1997b; *Stein et al*., 1997; *Nalbant et al*., 1998; *King et al*., 2001]. In these studies, the Coulomb failure criterion is widely used to describe the static conditions under

which rocks fail. In this framework, faults with a given orientation and preferential slip direction fail when Coulomb failure stress (ΔCFS) is greater than

$$\Delta\text{CFS} = \Delta\tau - \mu'\Delta\sigma_n, \quad (1)$$

where $\Delta\tau$ is the shear stress change on the plane and $\Delta\sigma_n$ is the normal stress change on the plane with compression defined as positive, and $\mu\prime$ is the effective coefficient of friction [e.g., *King et al*., 1994]. The effective coefficient of friction $\mu\prime$ (equation (1)) assumes that fluid pressure is linearly related to the confining stress on the failure plane. Positive ΔCFS values have also been used to successfully explain aftershocks locations in some cases, such as after the Landers earthquake [*Hardebeck et al*., 1998] and the 1989 $M_W = 7.1$ Loma Prieta earthquake [*Parsons et al*., 1999]. However, the spatial correlation between aftershock locations and positive ΔCFS is not always clear; static stress triggering cannot explain the locations of aftershocks in the month after the 1994 $M_W = 6.7$ Northridge earthquake significantly better than it can explain synthetic random distributions of aftershocks [*Hardebeck et al*., 1998]. In addition, static stress transfer occurs instantaneously, and thus cannot easily explain time delays of years to decades between a main event and subsequent triggered events without incorporating additional statistical or physical modeling techniques, such as rate and state friction [e.g., *Stein et al*., 1997; *Parsons et al*., 2000].

Dynamic stresses, or stresses induced by the passage of seismic waves, may be more likely to effect far-field seismicity rates than static stress changes. The magnitudes of static stress changes decrease as $1/r^3$, where r is the distance from a finite source [*Okada*, 1992], while the magnitudes of dynamic stresses decay more gradually, as $1/r$. As a result, dynamic stresses have been used to explain the sudden and dramatic increases in seismicity rates observed across the western United States after the Landers, Hector Mine, and Denali earthquakes [e.g., *Hill et al*., 1993; *Anderson et al*., 1994, *Gomberg et al*., 2001, 2004; *Eberhart-Phillips et al*., 2003, *Prejean et al*., 2004; *Brodsky and Prejean*, 2005]. In the near field, the locations of aftershocks of the Landers earthquake are also correlated with the areas of highest transient ΔCFS due to seismic waves [*Kilb et al*., 2000, 2002]. However, dynamic stresses are transient and pass through the crust within hours of a large earthquake, and thus can only provide a direct mechanism to trigger aftershocks [e.g., *Kilb et al*., 2000, 2002] or far-field earthquakes [e.g., *Pollitz et al*., 2012; *Gonzalez-Huizar et al*., 2012] in a short time window (<1 day) after an earthquake.

A number of secondary mechanisms have been proposed to explain long (>1 day) delays between earthquakes. Rate and state friction [e.g., *Dieterich*, 1992, 1994], subcritical crack growth [*Atkinson*, 1984], and transient increases in pore pressures [e.g., *Brodsky et al*., 2003; *Hill et al*., 1993] have been invoked to explain earthquake triggering with longer time delays of days, weeks, and years. However, the locations and times of remotely triggered earthquakes in the Long Valley suggest a frequency-dependent threshold, which may not be consistent with rate and state friction or subcritical crack growth models [*Brodsky and Prejean*, 2005; *Freed*, 2005].

Stress transfer by viscoelastic relaxation of the lower crust and upper mantle is a mechanism for which a delay of years to decades between the "triggering" earthquake and the "triggered" earthquake might be expected. The triggering earthquake may generate diffusive viscoelastic fronts within the upper mantle that slowly increase or decrease ΔCFS in the surrounding crust. This mechanism of stress transfer has been used to explain the delayed triggering of the Hector Mine earthquake 7 years after the Landers earthquake [*Freed and Lin*, 2001; *Zeng*, 2001; *Pollitz and Sacks*, 2002], the 1944 $M_W = 8.0$ Tonankai, 1946 $M_W = 8.2$ Nankaido, and 1995 $M_W = 6.9$ Kobe earthquakes in Japan [*Pollitz and Sacks*, 1997], the 1905 $M_W = 7.9$ Tsetserleg and $M_W = 8.4$ Bolnai earthquakes, the 1931 $M_W = 8.0$ Fu Yun earthquake, the 1957 $M_W = 8.1$ Gobi-Altai earthquake, and the 1967 $M_W = 7.1$ Mogod earthquakes in Mongolia [*Pollitz et al*., 2003], and the triggering of oceanic intraplate earthquakes by large interplate earthquakes along the Aleutian arc [*Pollitz et al*., 1998]. Other time-dependent stress transfer mechanisms, such as time-dependent afterslip and poroelastic rebound, have been suggested as possible explanations for delayed earthquake triggering on shorter (<5 year) timescales [e.g., *Jónsson et al*., 2003; *Bürgmann et al*., 2002].

Along the NAF (Figure 1), viscoelastic stress transfer was first proposed over two decades ago [*Roth*, 1988; *Tselentis and Drakopoulos*, 1990]. More recently, a linear Maxwell rheology was used to explain the 1939–1999 earthquake sequence along the North Anatolian fault; at eight out of nine of the earthquake epicenters, ΔCFS values due to the previous earthquakes in the sequence were positive [*Lorenzo-Martín et al*., 2006]. To

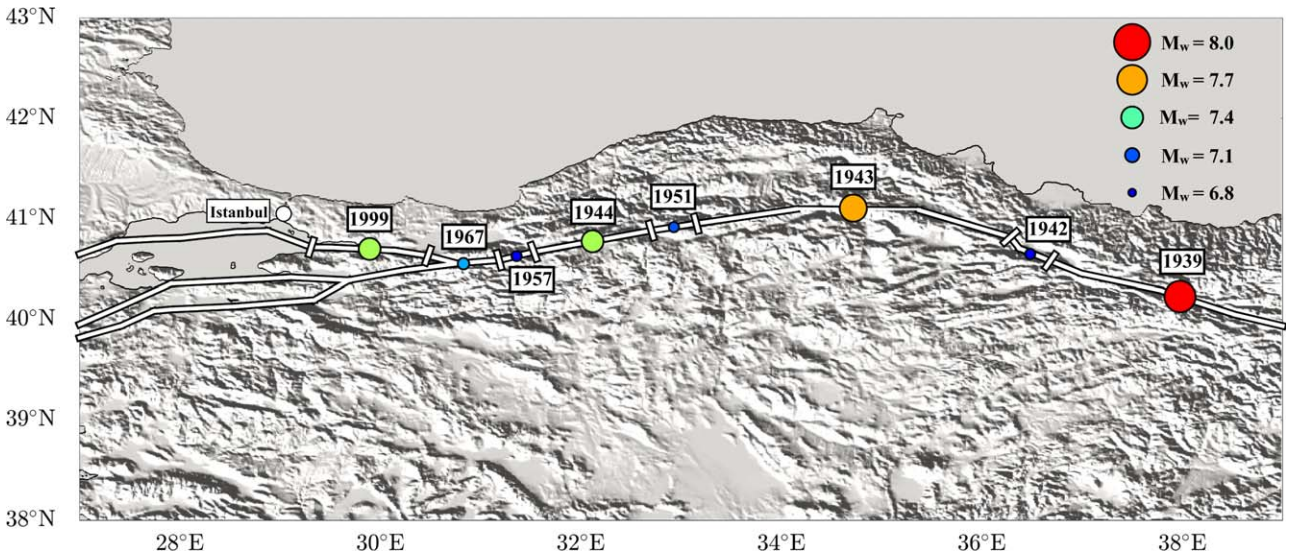

Figure 1. Map of the locations and sizes of the historic earthquakes in the 1939–1999 earthquake sequence. The detailed model parameters of these earthquakes are listed in detail in Table 1.

estimate ΔCFS values, these authors used a multilayered geometry (three elastic and two viscoelastic layers) with linear Maxwell rheologies in the two deepest layers.

However, geodetic data from before and after the $M_W = 7.4$ Izmit earthquake along the NAF suggest that a two-layer Maxwell rheology is insufficient to simultaneously explain fast transient postseismic velocities (>100 mm/yr) and a differential velocity across the fault (~24 mm/yr over a 200 km fault-perpendicular transect) late in the earthquake cycle [*Hetland*, 2006; *Hearn et al*., 2002a]. This has also been suggested in subsequent three-dimensional studies of postseismic deformation in Turkey [*Hearn et al*., 2002b, 2009]. Similar geodetic observations from before and after the 2001 $M_W = 7.8$ Kokoxili earthquake [*Zhang et al*., 2004; *Ryder et al*., 2007, 2011] and the 1997 M_W=7.6 Manyi earthquake [*Bell et al*., 2011; *ChaoJun et al*., 2009] in Tibet also suggest that two-layer Maxwell rheologies may be insufficient to explain all available geodetic data. However, multilayer models incorporating Maxwell rheologies [*Hetland and Hager*, 2006; *Hetland*, 2006] may be able to explain data from the entire earthquake cycle more completely than two-layer Maxwell models [*DeVries and Meade*, 2013].

Two sets of models that may be able to explain both pre-earthquake and post-earthquake geodetic observations incorporate either viscous shear zones [e.g., *Yamasaki et al*., 2014; *Hearn and Thatcher*, 2015] or Burgers rheologies [e.g., *Hetland*, 2006]. In particular, models that incorporate Burgers rheologies can explain pre-earthquake and post-earthquake data from both the NAF [*Hetland*, 2006] and 15 strike slip faults worldwide in two dimensions [*Meade et al*., 2013], and may also be consistent with time-dependent spatial patterns of far-field seismic activity after large earthquakes [*Marsan and Bean*, 2003]. Burgers viscoelastic rheologies explicitly incorporate two relaxations times and are often schematically represented as a Maxwell body in series with a Kelvin-Voigt body (Figure 2). Along the NAF, a two-layer Burgers model with a transient (Kelvin) relaxation timescale ($\tau_K = \frac{\eta_K}{\mu_K}$) of 2–5 years (or η_K=0.8 × 10^{18} − 1.9 × 10^{18} Pa·s for μ_K=3 × 10^{10} Pa) and a long-term (Maxwell) timescale ($\tau_M = \frac{\eta_M}{\mu_M}$) of over 400 years ($\eta_M \approx 1.5 \times 10^{20}$ Pa·s for μ_K=3 × 10^{10} Pa) can explain the pre-earthquake and post-earthquake geodetic observations from the 1999 M_W= 7.4 Izmit earthquake [*Hetland*, 2006] in two dimensions. However, to explain a given magnitude of surface deformation, a three-dimensional viscoelastic model must incorporate lower viscosities than two-dimensional models [e.g., *Hetland and Hager*, 2003]. In three dimensions, the postseismic GPS velocity field alone has been explained by stable frictional afterslip in the first few months after the earthquake and viscoelastic deformation with a Maxwell model with a viscosity of 2−5 ×10^{19} Pa·s [*Hearn et al*., 2009]. In order to explain both fast postseismic motions and the velocities across the fault late in the earthquake cycle, these authors discuss how a Maxwell rheology would be insufficient, and a Burgers rheology (with viscosities 2−5 × 10^{19} Pa·s and at least 2 × 10^{20} Pa·s) may be required in addition to stable afterslip [*Hearn et al*., 2009]. In a more recent study [*DeVries et al*., 2014] a two-dimensional grid search across viscosity

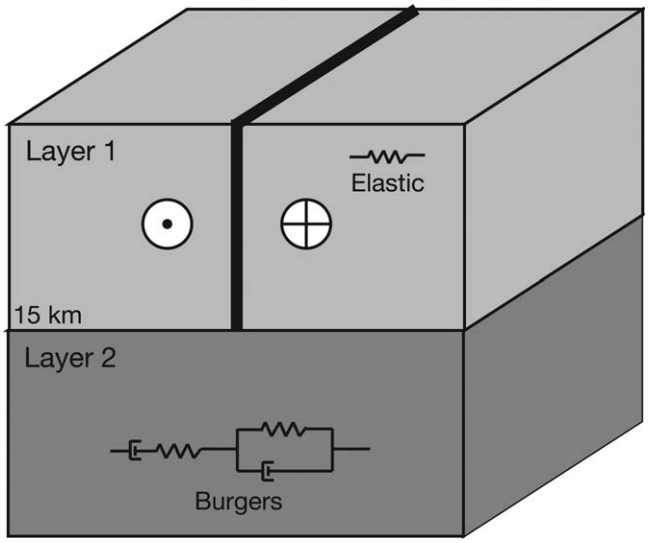

Figure 2. The geometry and rheologies used in this study.

structures was conducted in order to find viscosities that allow a two-layer (crust and mantle) Burgers model to best explain (1) a 7 year post-Izmit time series from GPS station TUBI (η_M=4 × 10^{18} Pa s and η_K=1 × 10^{18} Pa s) [*Ergintav et al.*, 2009] and (2) the pre-Izmit velocity field with viscoelastic block models ($\eta_M = 1 \times 10^{19}$ Pa s and $\eta_K = 1 \times 10^{19}$ Pa s). This previous study suggests that the available data from both before and after the Izmit earthquake may be explained in three dimensions by a two-layer Burgers model with a Maxwell viscosity of $\eta_M = 4 \times 10^{18} - 1 \times 10^{19}$ Pa s and a Kelvin viscosity of $\eta_K = 1 \times 10^{18} - 1 \times 10^{19}$ Pa s.

Here, using this geodetically constrained range of Burgers rheologies, we examine the predicted time evolution of Coulomb failure stress changes (ΔCFS) along the North Anatolian fault due to viscoelastic stress transfer and compare the apparent mean threshold values of ΔCFS at which the earthquakes in the sequence occur (~0.02–3.15 MPa).

2. Earthquake History Along the NAF

The North Anatolian fault has ruptured in a series of eight $M_W > 6.7$ westward propagating earthquakes in 1939, 1942, 1943, 1944, 1951, 1957, 1967, and 1999 (Figure 1 and Table 1) [*Barka*, 1992, 1996; *Stein et al.*, 1997]. Historical records suggest that 1939-like earthquakes may have occurred in 1254 and 1045, a 1943-like earthquake may have occurred in 1668, and 1957, 1944, and 1951-like earthquakes may have occurred in 967, 1035, and 1050 [*Barka*, 1996]. The records of historic earthquakes along the central and eastern NAF (31–39° longitude) suggest that earthquake sequences like the 1939–1999 sequence could have occurred in the past [*Barka*, 1996]. The historic earthquakes included in the stress calculations, and their parameters, are listed in Table 1. Although the 1951 earthquake likely re-ruptured segments of the fault that had previously ruptured in the 1944 earthquake [*Barka*, 1996], we have simplified the geometry of these earthquakes so that the two ruptures do not overlap. We also neglect the effects of the 1992 earthquake as it occurred to the east of our study area (Figure 1) and the 1999 M_W=7.2 Düzce earthquake as it occurred along segments not included in the viscoelastic block model [*DeVries et al.*, 2014].

Roman, Byzantine, and Ottoman written records from present-day Turkey suggest the occurrence of 55 $M \geq 6.8$ earthquakes since 0 AD in the Sea of Marmara region [*Ambraseys*, 2002]. Here we focus on the effects of the 1939–1999 sequence because they have induced the most recent stress changes along the fault system.

Table 1. The Parameters of the Eight Earthquakes Included in the Models of Stress Transfer

Earthquake	Length of rupture (km)	M_0 (Nm)	M_W	Average slip (m)	References
26 Dec 1939	263	4.11 × 10^{20}	7.7	3.47	1, 2, and 3
20 Dec 1942	44	1.74 × 10^{19}	6.8	0.88	1, 2, and 3
26 Nov 1943	270	2.51 × 10^{20}	7.6	2.07	1, 2, and 3
1 Feb 1944	101	1.48 × 10^{20}	7.4	3.24	1, 2, and 3
13 Aug 1951	38	2.12 × 10^{19}	6.9	1.22	1, 2, and 3
26 May 1957	31	1.35 × 10^{19}	6.7	0.98	1, 2, and 3
22 Jul 1967	61	2.82 × 10^{19}	7.0	1.02	1, 2, and 3
19 Aug 1999	99	1.26 × 10^{20}	7.4	2.83	4

[1]*Barka* [1992], [2]*Barka* [1996], [3]*Lorenzo-Martín et al.* [2006], [4]*Barka* [1999].

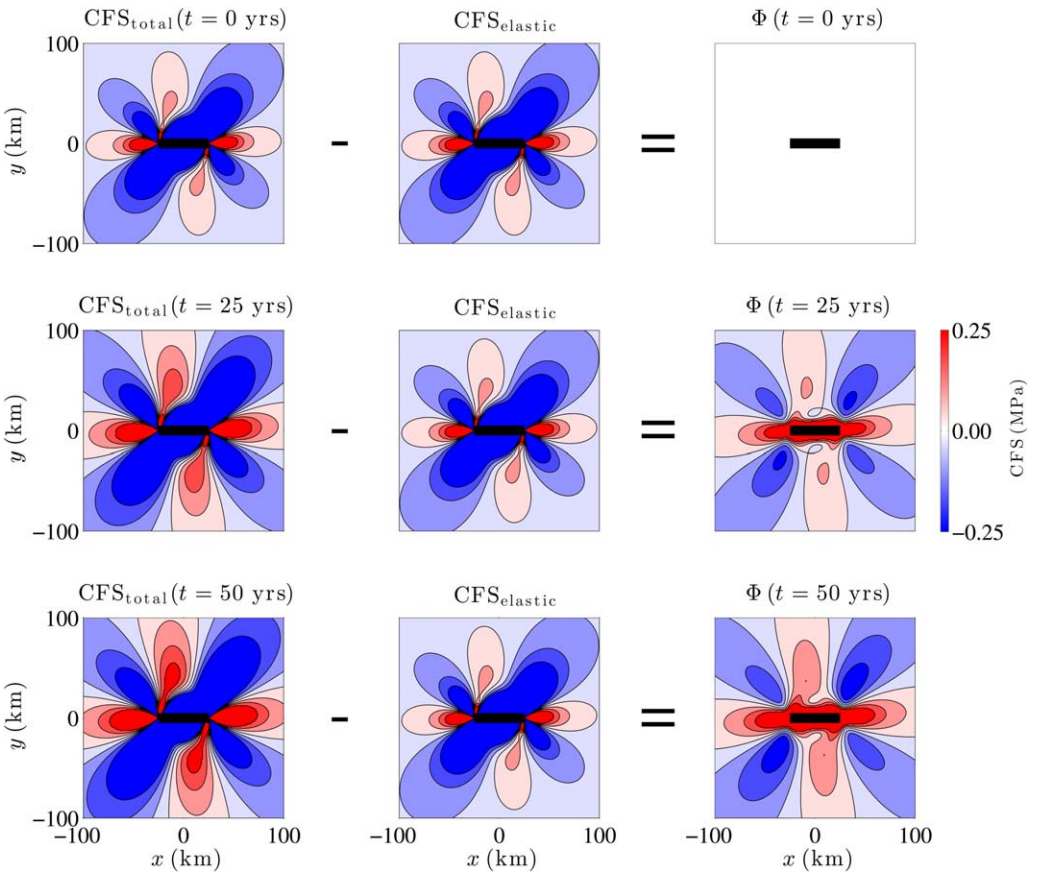

Figure 3. The components of $\phi(t)$ (equation (2)) for a two-layer Maxwell model with a Maxwell viscosity of $\eta_M = 1 \times 10^{19}$ Pa s at three times (0, 25, and 50 years) after an idealized earthquake of $M_W = 7.3$. The idealized fault is 50 km long, it ruptures to 15 km depth, and slip is assumed to be a uniform 5 m.

Previous stress transfer modeling studies of the 1939–1999 NAF earthquake sequence [*Stein et al.*, 1997; *Lorenzo-Martín et al.*, 2006] have also included the effects of a steady background stress. We do not include the effects of such a background tectonic stress here, as our primary goal is to understand how historic earthquakes may modulate any steady stress accumulation patterns.

3. $\phi(t)$: The Viscoelastic Component of Coulomb Failure Stress

Viscoelastic diffusion of coseismic stresses inherently leads to time-dependent stresses in the crust that may vary over years, decades, or centuries. The time-dependent component of stress change due to viscoelastic relaxation only, excluding step changes associated with coseismic elastic effects, may be an important quantity to consider when explaining the timing, magnitude, and locations of triggered earthquakes. Here we denote this quantity as $\phi(t)$ (Figure 3) for fixed receiver fault geometries

$$\phi(t) = \Delta\mathrm{CFS}_{\mathrm{total}}(t) - \Delta\mathrm{CFS}_{\mathrm{elastic}}. \tag{2}$$

Immediately after a single earthquake, $\phi(t)=0$ everywhere because $\Delta\mathrm{CFS}_{\mathrm{total}}(t=0) = \Delta\mathrm{CFS}_{\mathrm{elastic}}$ (Figure 3). However, the large stresses generated by the earthquake at the base of the seismogenic zone induce rapid viscoelastic relaxation in the layer below, reloading the fault and leading to increases in the magnitude of $\phi(t)$ along planes parallel to the fault. The largest off-fault values of $\Delta\mathrm{CFS}_{\mathrm{total}}(t)$ and $\phi(t)$ occur at the terminations of the rupture (Figure 3). For an idealized $M_W = 7.3$ rupture (Figure 3) and a two-layer Maxwell model ($\eta_M = 1 \times 10^{19}$ Pa s), after 50 years, at locations 20 km east and west of the fault tip at 10 km depth, $\phi(t=50) = 0.44$ MPa, which represents a 91% increase in $\Delta\mathrm{CFS}_{\mathrm{total}}(t=50)$ over $\Delta\mathrm{CFS}_{\mathrm{elastic}}$ (Figure 3).

The calculations of $\Delta CFS_{total}(t)$ and $\phi(t)$ in this paper use a spectral propagator matrix approach for calculating strains, stresses, velocities, and displacements [*Sato*, 1971; *Sato and Matsu'ura*, 1973, 1988; *Matsu'ura and Sato*, 1975, 1989; *Fukahata and Matsu'ura*, 2005, 2006; *Hashima et al*., 2014]. The approach [*Fukahata and Matsu'ura*, 2005, 2006] can incorporate an arbitrary number of viscoelastic layers with Maxwell rheologies using the correspondence principle, which allows any linear viscoelastic problem to be written in the form of an elastic problem in the Laplace domain [e.g., *Nur and Mavko*, 1974; *Savage and Prescott*, 1978; *Hetland and Hager*, 2006; *de Hoog et al*., 1982]. Here, we incorporate Burgers rheologies and use a numerical inverse Laplace transform [*de Hoog et al*., 1982; *Hollenbeck*, 1998]. We also use the simple two layer geometry and rheology constrained by geodetic data along the NAF [*DeVries et al*., 2014] in which faults extend to the base of the elastic layer at 15 km depth (Figure 2).

4. Results

4.1. $\Delta CFS(t)$ and $\phi(t)$ Across Anatolia from 1939 to 1999

To understand the full range of possible time-dependent stress evolution patterns, we perform all calculations for the two end-member cases. We will refer to these end-member viscosity structures as VS1 ($\eta_M = 4 \times 10^{18}$ Pa s, $\eta_K = 1 \times 10^{18}$ Pa s) and VS2 (l$\eta_M = 1 \times 10^{19}$ Pa s, η_K=1×10^{19} Pa s). Because the NAF fault system consists of largely east-west striking faults, $\Delta CFS(t)$ values are plotted with respect to east-west striking vertical receiver planes in map view (Figure 4 and supporting information Figure A1). Values of $\Delta CFS(t)$ and $\phi(t)$ represent the compounded effects of all earthquakes since 1939.

As might be expected based on calculations with an idealized fault (Figure 3), $\Delta CFS(t)$ (Figure 4 and supporting information Figure A1) and $\phi(t)$ (Figure 5 and supporting information Figure A2) values at 10 km depth on vertical east-west striking receiver planes during the 1939–1999 earthquake sequence are highest in well-defined lobes at the tips of recently ruptured fault segments. Across the two end-member viscosity structures, lobes of $\phi(t) > 0.01$ MPa extend ~0–325 km west of the tip of the most recent earthquake rupture at the time of the next earthquake (Figure 5 and supporting information Figure A2). At the time of the 1944 earthquake, a positive lobe $\phi(t) > 0.01$ MPa extended between ~0 and 62 km (VS2–VS1) to the west of the 1943 rupture at 10 km depth (Figure 5 and supporting information Figure A2). At the times of the other earthquakes, lobes of $\phi(t) > 0.01$ MPa extended up to ~78% farther toward the west along the fault system with the lower viscosity end-member case (VS1) than with the higher viscosity end-member case (VS2; Figure 5 and supporting information Figure A2). This pattern might be expected as stresses due to viscoelastic relaxation diffuse more rapidly at lower viscosities [e.g., *Savage and Prescott*, 1978].

4.2. $\Delta CFS(t)$ and $\phi(t)$ Resolved Along the NAF from 1939 to 2020

To investigate delayed earthquake triggering along the NAF from 1939-present, the most important quantities to examine may be $\Delta CFS(t)$ and $\phi(t)$ resolved on the vertical fault planes immediately before each earthquake at 10 km depth. Here t_{eq}^{-} denotes the time immediately before each earthquake (Table 2 and Figure 6). In particular, estimates of $\Delta CFS^{\{h\}}(t_{eq}^{-})$ (supporting information Figure A5) and $\phi^{\{h\}}(t_{eq}^{-})$ (supporting information Figure A3) at the earthquake hypocenters and the mean values $\overline{\Delta CFS}(t_{eq}^{-})$ (supporting information Figure A4) and $\overline{\phi}(t_{eq}^{-})$ (Figure 6) at 10 km depth could provide information about apparent earthquake triggering thresholds. We exclude locations less than 6 km from the recently ruptured segments in these calculations. Below we summarize some particularly interesting aspects of these results (Figure 6 and supporting information Figure A3–A5).

1. The estimated mean of the values of $\overline{\phi}(t_{eq}^{-})$ for all seven earthquakes in the 1939–1999 sequence, $\overline{\phi}(t_{eq}^{-})$, ranges from ~0.13 MPa (VS2) to ~0.21 MPa (VS1; Table 2 and Figure 6). Locally, at the hypocenters of the earthquakes, the mean value of $\phi^{\{h\}}(t_{eq}^{-})$ across all seven earthquakes, $\phi^{\{h\}}(t_{eq}^{-})$, ranges from 0.11 MPa (VS2) to 0.18 MPa (VS1; supporting information Figure A3).
2. These bulk statistics do not fully represent the complexity of the results (Figure 6 and supporting information Figure A3). While the values of $\overline{\phi}(t_{eq}^{-})$ and $\phi^{\{h\}}(t_{eq}^{-})$ at 10 km depth are positive prior to all seven earthquakes in the 1939–1999 earthquake sequence (Table 2 and Figure 6), the individual magnitudes of $\overline{\phi}(t_{eq}^{-})$ and $\phi^{\{h\}}(t_{eq}^{-})$ vary by two orders of magnitude (Table 2 and Figure 6). Across the range of end-member viscosity structures, $\overline{\phi}(t_{eq}^{-})$ values are estimated to be as small as ~0.002 MPa (1944 earthquake) and as large as ~0.564 MPa (1951 earthquake). Similarly, the local magnitudes of $\phi^{\{h\}}(t_{eq}^{-})$ at the hypocenters of the earthquakes vary from ~0.002 MPa (1943 earthquake) to ~0.598 MPa (1951

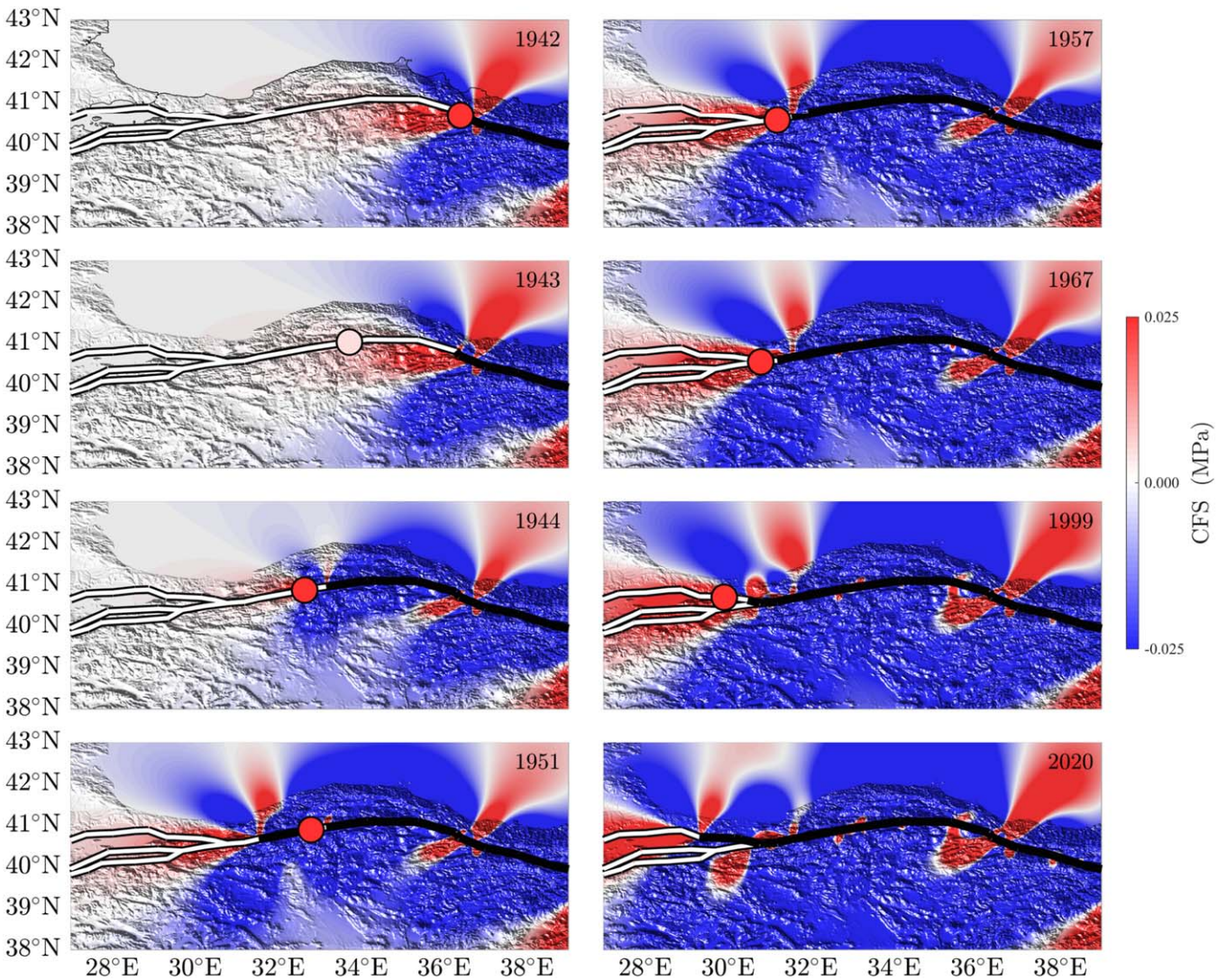

Figure 4. Maps of estimated $\Delta CFS_{total}(t)$ at 10 km depth on the day before the 1942, 1943, 1944, 1951, 1957, 1967, and 1999 earthquakes for end-member viscosity structure VS1 ($\eta_M = 4 \times 10^{18}$ Pa s, $\eta_K = 1 \times 10^{18}$ Pa s). Projected map of $\Delta CFS_{total}(t)$ in 2020 in the absence of additional earthquakes is also included. Because the NAF fault system consists of largely east-west striking faults, $\Delta CFS(t)$ changes are plotted with respect to vertical east-west striking receiver planes. Analogous figure for end-member viscosity structure VS2 ($\eta_M = 1 \times 10^{19}$ Pa s, $\eta_K = 1 \times 10^{19}$ Pa s) is included in supporting information Figure A1. Circles, colored by local $\Delta CFS(t)$ value resolved on the fault, highlight the location of the next earthquake in the sequence.

earthquake). Overall, the large magnitude variations in $\overline{\phi}(t_{eq}^-)$ and $\phi^{\{h\}}(t_{eq}^-)$ across the earthquakes suggests that there is not a straightforward correlation between magnitude of $\overline{\phi}(t_{eq}^-)$ or $\phi^{\{h\}}(t_{eq}^-)$ and the timing of the ruptures.

3. The values of $\Delta CFS(t_{eq}^-)$ at 10 km depth may be important quantities to examine in addition to $\phi(t_{eq}^-)$ values [e.g., *Lorenzo-Martín et al.*, 2006]. The universal mean, $\overline{\Delta CFS}(t_{eq}^-)$, across all of the earthquakes is estimated to be between ~0.70 MPa (VS2) and ~0.77 MPa (VS1; Table 2 and supporting information Figure A4). At the earthquake hypocenters, the mean value of $\Delta CFS^{\{h\}}(t_{eq}^-)$ across all earthquakes, $\overline{\Delta CFS}^{\{h\}}(t_{eq}^-)$, is estimated to be between ~0.42 MPa (VS2) and ~0.49 MPa (VS1; Table 2 and supporting information Figure A4).
4. The individual magnitudes of $\overline{\Delta CFS}(t_{eq}^-)$ along each rupture plane vary significantly across the seven earthquakes (Table 2 and supporting information Figure A4). Prior to all earthquakes, the mean values of $\overline{\Delta CFS}(t_{eq}^-)$ along the earthquake rupture lengths are positive (~0.020 to ~3.153 MPa; supporting information Figure A4). Values of $\Delta CFS^{\{h\}}(t_{eq}^-)$ are also positive for all earthquakes (~0.003 to ~2.205 MPa, supporting information Figure A5).

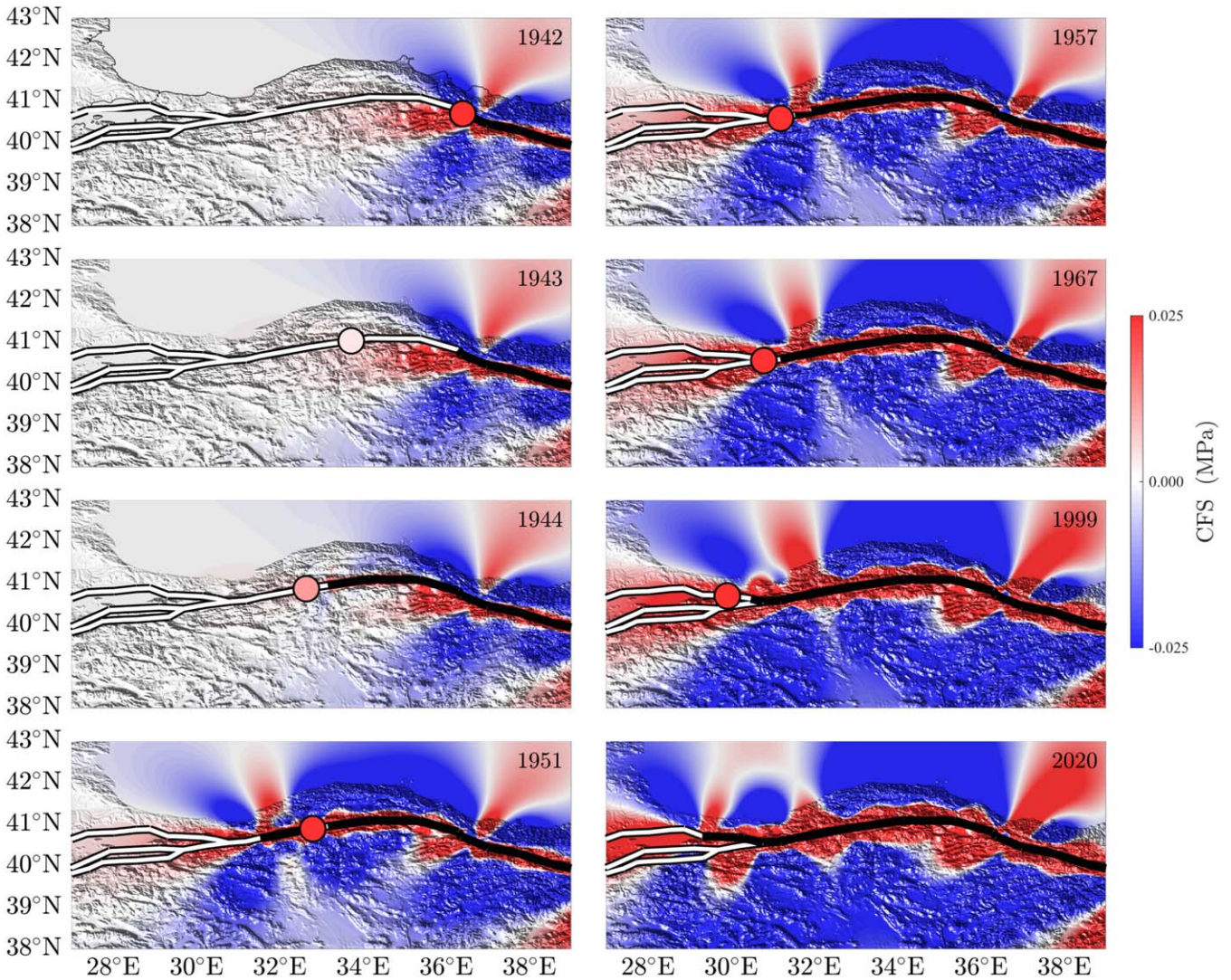

Figure 5. Maps of estimated $\phi(t)$ at 10 km depth on the day before the 1942, 1943, 1944, 1951, 1957, 1967, and 1999 earthquakes for end-member viscosity structure VS1 ($\eta_M = 4 \times 10^{18}$ Pa s, $\eta_K = 1 \times 10^{18}$ Pa s). Projected map of $\phi(t)$ in 2020 in the absence of additional earthquakes is also included. Because the NAF fault system consists of largely east-west striking faults, $\phi(t)$ changes are plotted with respect to vertical east-west striking receiver planes. Analogous figure for end-member viscosity structure VS2 ($\eta_M = 1 \times 10^{19}$ Pa s, $\eta_K = 1 \times 10^{19}$ Pa s) is included in supporting information Figure A2. Circles, colored by local $\phi(t)$ value resolved on the fault, highlight the location of the next earthquake in the sequence.

5. The smallest (<0.10 MPa) apparent stress change thresholds are associated with the 1943 and 1944 earthquakes. For the 1943 earthquake, calculated local $\Delta\text{CFS}^{\{h\}}(t_{eq}^-)$ values at the earthquake hypocenters are only ~0.003–0.006 MPa, while mean values of $\overline{\Delta\text{CFS}}(t_{eq}^-)$ for this earthquakes may be larger (~0.03–0.04 MPa). Values of $\overline{\phi}(t_{eq}^-)$ and $\phi^{\{h\}}(t_{eq}^-)$ follow a similar pattern for this 1943 event: $\overline{\phi}(t_{eq}^-)$ is estimated to be ~0.007–0.017 MPa and $\phi^{\{h\}}(t_{eq}^-)$ is estimated to be ~0.002–0.004 MPa.

   For the 1944 earthquake, estimated local $\Delta\text{CFS}^{\{h\}}(t_{eq}^-)$ values at the earthquake hypocenter are ~0.06–0.07 MPa and estimated mean values of $\overline{\Delta\text{CFS}}(t_{eq}^-)$ are similar magnitudes (~0.020–0.025 MPa). However, for this 1944 event, estimated $\overline{\phi}(t_{eq}^-)$ values are only ~0.002–0.007 MPa and estimated $\phi^{\{h\}}(t_{eq}^-)$ values are ~0.003–0.012 MPa. Small (<0.10 MPa) apparent stress change threshold values due to both elastic and viscoelastic effects for the 1943 and 1944 earthquakes may be expected, because these earthquakes occur shortly after (<1 year) and at relatively large epicentral distances (>~50 km) from previous earthquakes.
6. The largest magnitude $\overline{\phi}(t_{eq}^-)$ and $\overline{\Delta\text{CFS}}(t_{eq}^-)$ values of all seven earthquakes ($\overline{\phi}(t_{eq}^-) = 0.365$–$0.564$ MPa and $\overline{\Delta\text{CFS}}(t_{eq}^-) = 2.954$–$3.153$ MPa) occur along the 1951 earthquake rupture length (Table 2, Figure 6,

Table 2. The Quantities $\overline{\phi}(t_{eq}^{-})$, $\phi^{\{h\}}(t_{eq}^{-})$, $\overline{\Delta CFS}(t_{eq}^{-})$, and $\Delta CFS^{\{h\}}(t_{eq}^{-})$ in Units of MPa for this Study and the Previous Viscoelastic Study of the NAF Earthquake Sequence [*Lorenzo-Martín et al.*, 2006, Table 2].

Earthquake	$\overline{\phi}(t_{eq}^{-})$ (this study)	$\overline{\phi}(t_{eq}^{-})$ (Reference 1[a])	$\phi^{\{h\}}(t_{eq}^{-})$ (this study)	$\overline{\Delta CFS}(t_{eq}^{-})$ (this study)	$\overline{\Delta CFS}(t_{eq}^{-})$ (Reference 1[a])	$\Delta CFS^{\{h\}}(t_{eq}^{-})$ (this study)
1942	0.087–0.202	0.01–0.19	0.066–0.156	0.571–0.686	(−0.66)– (−0.48)	0.291–0.381
1943	0.007–0.017	0.01–0.03	0.002–0.004	0.028–0.039	0.05–0.07	0.003–0.006
1944	0.002–0.007	0.00–0.01	0.003–0.012	0.020–0.025	0.36–0.37	0.058–0.068
1951	0.365–0.564	0.06–0.38	0.387–0.598	2.954–3.153	(−2.92)–(−3.30)	1.994–2.205
1957	0.265–0.370	0.04–0.14	0.152–0.217	0.878–0.982	0.90–1.00	0.321–0.386
1967	0.126–0.179	0.04–0.15	0.112–0.161	0.260–0.313	(−0.16)–(−0.27)	0.187–0.237
1999	0.092–0.128	0.04–0.11	0.072–0.102	0.165–0.200	0.37–0.44	0.098–0.128

[a]Includes effects of tectonic loading, [1]*Lorenzo-Martín et al.* [2006].

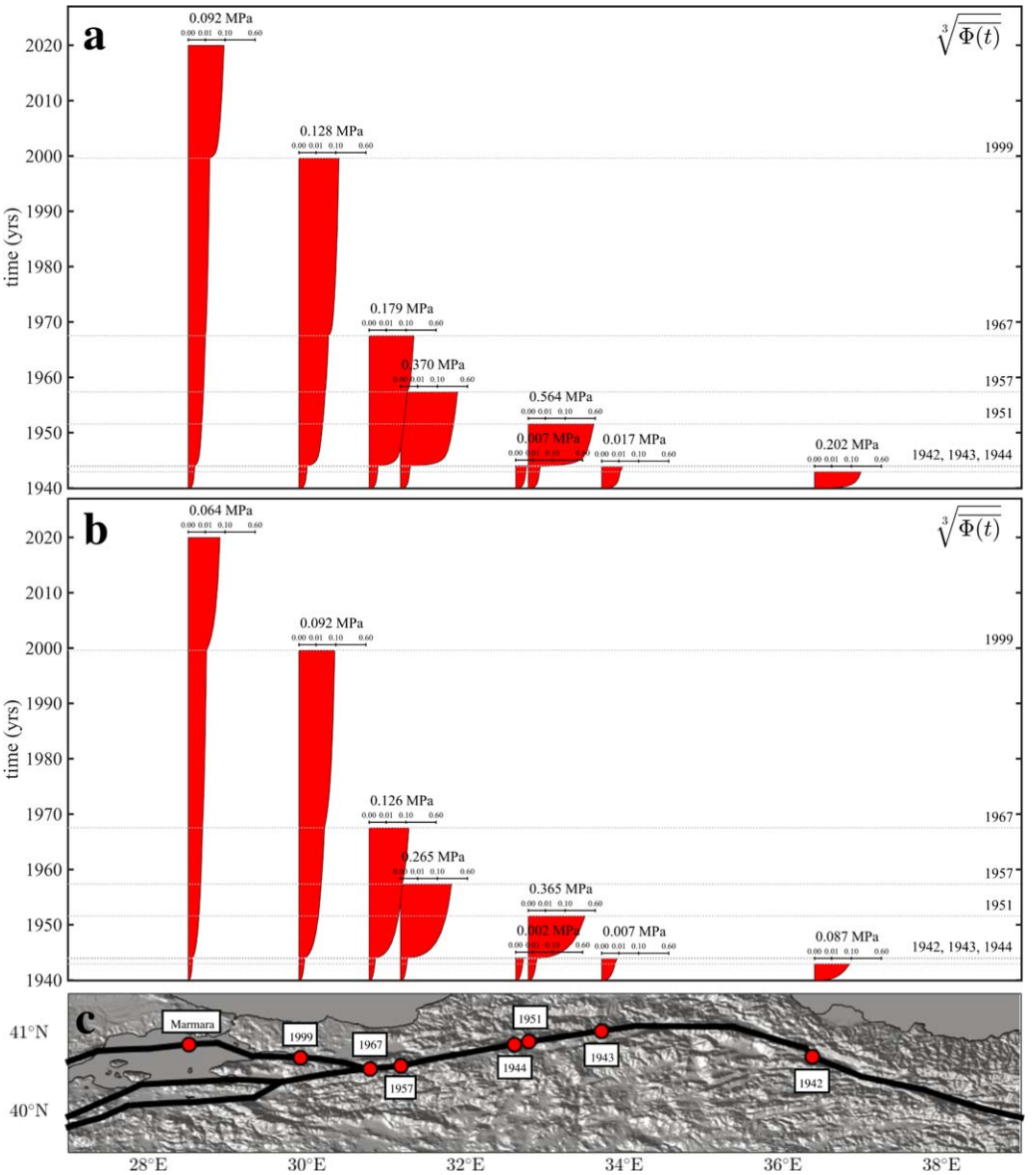

Figure 6. Evolution of third root of $\overline{\phi}(t)$ resolved along each earthquake rupture length at 10 km depth for (a) VS1 and (b) VS2. The third root of $\overline{\phi}(t)$ is plotted to emphasize small variations. Plotting the third root of $\overline{\phi}(t)$ is also physically appropriate because the magnitudes of static stress changes decrease as $1/r^3$. Dotted gray lines show the times of the earthquakes. The apparent threshold values of $\overline{\phi}\left(t_{eq}^{-}\right)$ immediately before each earthquake are printed above the curves.

and supporting information Figure A4). The 1951 earthquake likely re-ruptured segments of the NAF that had previously ruptured in 1944 [*Barka*, 1996]. However, for simplicity, we have shortened the extent of the 1951 event so that it does not overlap with the 1944. The high values of $\phi(t_{eq}^-)$ and $\Delta CFS(t_{eq}^-)$ at the 1951 epicenter may be due to these geometric simplifications.

7. Changes in the locations of the earthquake hypocenters may have significant effects on the evolution of $\phi(t)$. Across the end-member viscosity structures for the 1942 earthquake, $0.066<\phi^{\{h\}}(t_{eq}^-)<0.156$ MPa (supporting information Figure A3). However, if the hypocenter was located only ~10 km to the northwest, the estimated $\phi^{\{h\}}(t_{eq}^-)$ would be up to ~25% smaller in magnitude. By contrast, if the hypocenter was located only ~10 km to the southeast, the estimated $\phi^{\{h\}}(t_{eq}^-)$ would be ~50% larger in magnitude. Because 1942 earthquake occurred before the installation of widespread seismic networks, uncertainties in its epicentral location are likely to be large [e.g., *Barka*, 1996].
8. The percent differences between $\Delta CFS_{elastic}$ and total $\Delta CFS(t)$ may shed light on the potential importance of the role of viscoelastic relaxation on earthquake triggering. The final values of $\overline{\Delta CFS}(t_{eq}^-)$ (Table 2) were ~9–177% larger than $\overline{\Delta CFS}_{elastic}(t_{eq}^-)$ values (supporting information Table A1). On average, $\overline{\Delta CFS}(t_{eq}^-)$ was 49–79% (VS2–VS1; standard deviations of 45–57%) larger than $\overline{\Delta CFS}_{elastic}(t_{eq}^-)$. These large percentage increases in ΔCFS interseismically suggest that despite the tremendous variation in the geometries and length scales of the earthquakes, viscoelastic relaxation may have a significant influence on stress transfer and earthquake triggering along all of the ruptures in the 1939–1999 sequence.
9. The rates of change of $\overline{\phi}(t)$, $\frac{d\overline{\phi}(t_{eq}^-)}{dt}$, are positive prior to all seven earthquakes, suggesting that the faults are being gradually loaded due to viscoelastic relaxation when the earthquakes occur. Of all the earthquakes, the slowest $\frac{d\overline{\phi}(t_{eq})}{dt}$ loading rates are ~0.001 MPa/yr, along the 1999 Izmit rupture extent. The fastest $\frac{d\overline{\phi}(t_{eq})}{dt}$ loading rates are ~0.027–0.030 MPa/yr along the 1951 earthquake rupture.
10. In five out of seven earthquakes, more than 90% of the earthquake rupture length experienced $\phi(t_{eq}^-)>0.01$ MPa. The exceptions are the 1943 and 1944 earthquakes, for which $\phi(t_{eq}^-)>0.01$ MPa along ~28–29% and <~11%, respectively, of the rupture lengths; small $\phi(t_{eq}^-)$ values for the 1944 earthquake in particular might be expected because the penultimate 1943 earthquake occurred only 4 months earlier and terminated more than 30 km away in these models.

4.3. ΔCFS(t) and ϕ(t) Along the North Anatolian Fault in the Marmara Sea From 1999 to 2100

The northernmost strand of the western NAF is often the focus of seismic hazard studies [e.g., *Parsons et al*., 1999; *Parsons*, 2004] in the Marmara Sea region because it runs <50 km from Istanbul and geodetic slip deficit rate estimates along it (24–29 mm/yr) are 3–9 times faster than along the southern strands (3–8 mm/yr) [*Reilinger and McClusky*, 2001, *Reilinger et al*., 2006; *Meade et al*., 2002].

Here we examine the evolution of $\phi(t)$ and $\Delta CFS(t)$ resolved along the northern strand of the NAF in the Marmara Sea in detail. The evolution of the mean values of $\phi(t)$ at 10 km depth along the rupture extents of the historical 1766 ($M_S = 7.1$), 1509 ($M_S = 7.2$), and 1912 ($M_S = 7.3$) earthquakes [*Ambraseys and Jackson*, 2000] suggest that the viscoelastic effects of the 1939–1999 earthquake sequence are currently loading the 1766 rupture extent by ~0.06 MPa per decade, the 1509 rupture extent by ~0.007–0.009 MPa per decade, and the 1912 rupture area by <0.005 MPa per decade (Figure 7). By 2020, between 81% (VS1) and 90% (VS2) of the entire northern strand in the Marmara Sea (the rupture extents of the 1766, 1509, and 1912 earthquakes together) may be loaded $\Delta CFS(t)>0.01$ MPa.

In particular, the viscoelastic effects of the 1999 earthquake appear to be significantly increasing the stress along the 1766 earthquake rupture extent. The mean static stress change ($\overline{\Delta CFS}_{elastic}$) due to the 1939–1999 earthquake sequence (~0.46 MPa) is only 48–50% of the projected value of $\overline{\Delta CFS}(t=2100)$ along this fault segment (~0.89–0.93 MPa). In 2015, $\overline{\phi}(t)$ along the 1766 rupture extent is estimated to be ~0.23–0.32 MPa, exceeding the ranges of the apparent triggering thresholds $\overline{\phi}(t_{eq}^-)$ of the 1942, 1943, 1944, 1967, and 1999 earthquakes and within the range of estimated $\overline{\phi}(t_{eq}^-)$ for the 1957 earthquake (Figure 7). Between 2003 and 2012, $\overline{\phi}(t)$ along the 1766 earthquake rupture extent exceeded the range of $\overline{\phi}(t_{eq}^-)$, the universal mean of the $\overline{\phi}(t_{eq}^-)$ values along the rupture lengths of the seven 1939–1999 earthquakes (Figure 7). In fact, after ~2023, the value of $\overline{\phi}(t_{eq}^-)$ along the 1766 rupture extent may exceed the apparent $\overline{\phi}(t_{eq}^-)$ triggering thresholds of all previous NAF earthquakes (Figure 7).

Along the more distant 1509 and 1912 rupture extents, static stress changes due to the 1939–1999 earthquake sequence are only ~7–12% of $\overline{\Delta CFS}(t=2100)$. Along the 1509 rupture extent, $\overline{\Delta CFS}(t=2100) =$

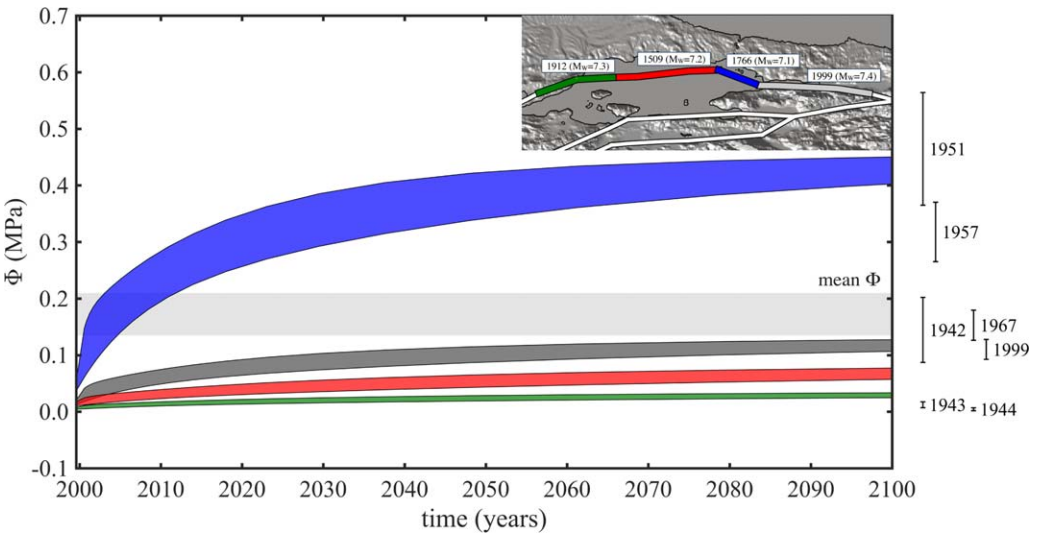

Figure 7. Evolution of $\overline{\phi}(t)$ resolved along the rupture lengths of the historical 1509 (red), 1912 (blue), and 1766 (green) earthquakes in the Sea of Marmara at 10 km depth. Curves are filled to show the ranges of the quantities defined by the two end-member viscosities VS1 and VS2. Filled gray rectangle shows the range of and then only the second quantity $\overline{\phi}(t_{eq}^{-})$ across the end-member viscosity cases. Bars on the far right labeled 1942, 1943, 1944, 1967, and 1999 indicate the individual ranges of $\overline{\phi}(t_{eq}^{-})$ for the earthquakes. Inset shows the western NAF in the Sea of Marmara, with the rupture extents of the 1509, 1766, and 1912 earthquakes highlighted.

0.06–0.08 MPa, while $\overline{\Delta CFS}_{elastic}(t{=}2100)$ is much smaller (~0.007 MPa). Similarly, along the 1912 rupture extent, $\overline{\Delta CFS}(t{=}2100)$= 0.03–0.04 MPa, while $\overline{\Delta CFS}_{elastic}(t{=}2100)$ is only ~0.003 MPa. Together these results suggest that viscoelastic relaxation may be a major contributor to total ΔCFS along the northern segments of the NAF in the Sea of Marmara.

While the evolution of mean values, $\overline{\phi}(t)$, along the 1509, 1766, and 1912 historical ruptures (Figure 7) provides useful geographical and historical context, it is also illuminating to examine the $\Delta CFS(t)$ and $\phi(t)$ at many locations along the northern strand of the NAF (Figure 8). This detailed examination of geographical variations in $\phi(t)$ from 1999 to 2100 (Figure 8) reveals that the largest local increases in ΔCFS after the 1999 Izmit earthquake is along the 1766 earthquake rupture, ~6 km from the tip of the 1999 earthquake. In this location, $\phi(t)$ reaches ~0.5 MPa by 2015 and >0.8 MPa by 2100. These large and positive values of $\phi(t)$ values exist only within a few kilometers of the 1999 rupture extent; ~8 km to the northwest, farther west along the 1766 rupture, $\phi(t)$ remains <0.5 MPa in 2100 (Figure 8). As might be expected, the values of $\phi(t)$ along the 1509 and 1912 earthquake ruptures are comparatively small (<0.10 MPa) due to their distance from the 1999 earthquake rupture (Figure 8).

5. Discussion

Thus far, we have emphasized the potential of viscoelastic relaxation to explain delayed earthquake triggering, because viscoelastic processes may lead to gradually increasing stress on nearby faults. However, viscoelastic relaxation also provides a mechanism to raise Coulomb failure stresses far from a fault, in regions where static Coulomb failure stress changes may be negligible because static stress changes decay as $1/r^3$ and $1/r^5$ from a finite source in a homogeneous elastic halfspace [*Okada*, 1992]. As discussed above, during the 1939–1999 NAF earthquake sequence, viscoelastic relaxation may have increased $\overline{\Delta CFS}$ noncoseismically by ~9–177%. Similar observations have been made in India and Mongolia, where calculated total increases in ΔCFS due to viscoelastic relaxation over 50–100 years were 4–7 [*To et al.*, 2004] or more [*Pollitz et al.*, 2003] times as large as static elastic stress changes at the hypocenters of nearby earthquakes.

Stresses as small as ~0.01 MPa have been correlated with locations of aftershocks in California, but it remains unclear if seismicity is correlated with ΔCFS smaller than ~0.01 MPa [*Harris*, 1998; *Nalbant et al.*, 1998; *Harris and Simpson*, 1996; *Deng and Sykes*, 1997b]. At the 1943 hypocenter, the magnitudes of $\phi^{\{h\}}(t_{eq}^{-})$ and $\Delta CFS^{\{h\}}(t_{eq}^{-})$ estimated here (~0.002 to 0.006 MPa) are significantly smaller than 0.01 MPa

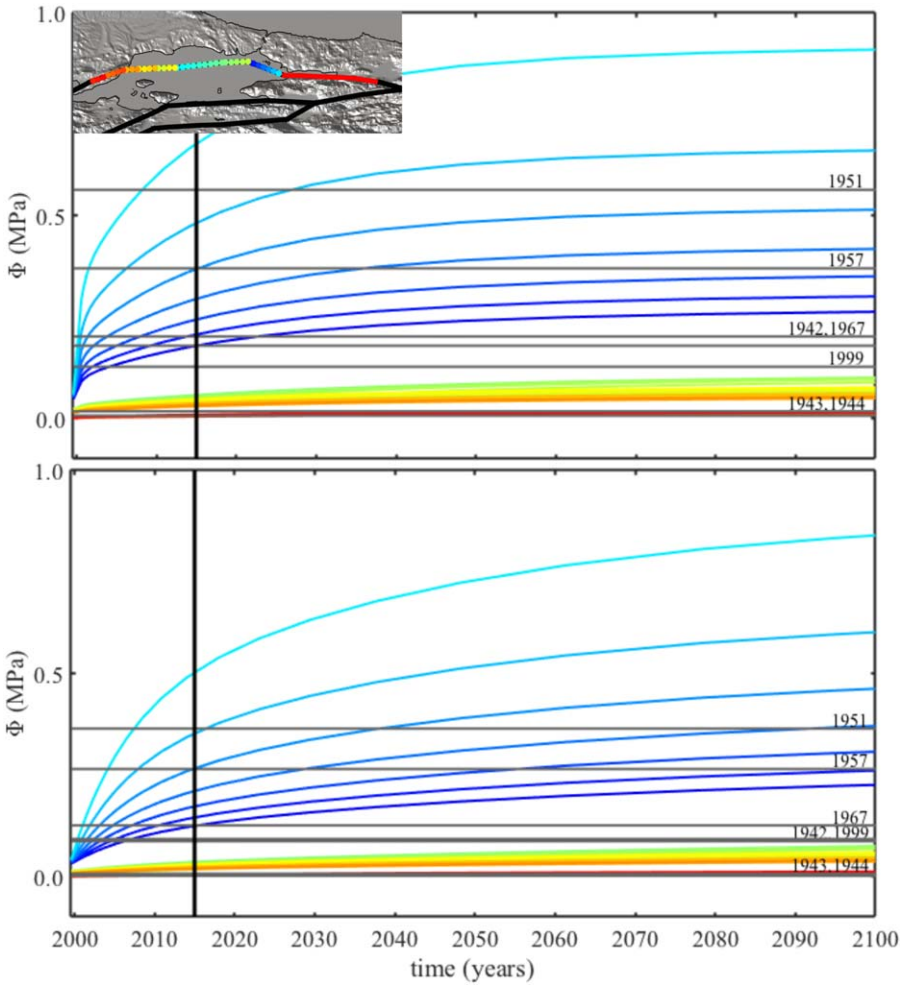

Figure 8. (top) Evolution of $\phi(t)$ resolved along the western NAF in the Sea of Marmara at 10 km depth with viscosity structure VS1 ($\eta_M = 4 \times 10^{18}$ Pa s, $\eta_K = 1 \times 10^{18}$ Pa s). (bottom) Analogous figure for VS2 ($\eta_M = 1 \times 10^{19}$ Pa s, $\eta_K = 1 \times 10^{19}$ Pa s). Gray lines indicate the $\overline{\phi}\left(t_{eq}^{-}\right)$ values for the 1942, 1943, 1944, 1951, 1957, 1967, and 1999 earthquakes along the NAF. Inset shows the western NAF in the Sea of Marmara, with individual points along the fault colored with the same color scheme as in Figures 8a and 8b.

(supporting information Figures A3 and A5). In fact, these values are comparable to the magnitudes of daily stress changes due to lunar tides (~0.002 MPa) [*Freed*, 2005; *Hill et al*., 1993]. Small stress changes such as those estimated along the 1943 and 1944 ruptures (Figure 6 and supporting information Figures A3–A5) could be dismissed as too small to contribute to earthquake triggering. Alternatively, quantities such as the loading rate $\frac{d\overline{\phi}(t)}{dt}$ or the percentage of the fault experiencing $\Delta\mathrm{CFS}(t) > 0$ MPa may be more important to consider in earthquake triggering studies.

Individual fault segments along the NAF fail at very different apparent thresholds of time-dependent earthquake-generated stress changes; values of $\overline{\phi}(t_{eq}^{-})$ and $\overline{\Delta\mathrm{CFS}}(t_{eq}^{-})$ (Figure 6 and supporting information Figure A4) both vary by up to two orders of magnitude (Table 2). However, the earthquakes in the 1939–1999 sequence do occur along fault segments that have experienced positive stress changes either coseismically, interseismically, or both: $\overline{\phi}(t_{eq}^{-})>0$ MPa and $\phi^{\{h\}}(t_{eq}^{-})>0$ MPa for all the earthquakes (Figure 6 and supporting information Figure A3), mean loading rates $\frac{d\overline{\phi}(t)}{dt}>0$ for all the earthquakes, and $\overline{\Delta\mathrm{CFS}}(t_{eq}^{-})>0$ MPa and $\Delta\mathrm{CFS}^{\{h\}}(t_{eq}^{-})>0$ MPa at all earthquake hypocenters (supporting information Figures A4 and A5). Thus, although the magnitudes of the ΔCFS changes vary along strike, the results do suggest that active faults in the NAF system experiencing positive values of $\overline{\phi}(t)$, $\overline{\Delta\mathrm{CFS}}(t)$, $\phi^{\{h\}}(t)$, $\Delta\mathrm{CFS}^{\{h\}}(t)$, or $\frac{d\overline{\phi}(t)}{dt}$ should be considered especially seriously in seismic hazard assessments.

The earliest viscoelastic studies of the NAF earthquake sequence [*Roth*, 1988; *Tselentis and Drakopoulos*, 1990] report shear stress changes ($\mu'=0$). In the first study [*Roth*, 1988], assuming a standard linear solid rheology, the mean shear stress estimated along the ruptures was more than 2.3 MPa prior to the earthquakes and noncoseismic changes in shear stress ranged from ~0.00 to 0.35 MPa. A second early study [*Tselentis and Drakopoulos*, 1990] assumed a two-layer Maxwell rheology and estimated non-coseismic changes in mean shear stress along the fault to be ~0.1–0.6 MPa.

A more recent study [*Lorenzo-Martín et al*., 2006] examined ΔCFS along the NAF during the 1939–1999 earthquake sequence using a layered Maxwell rheology. The magnitudes of $\overline{\phi}(t_{eq}^{-})$ estimated in this previous study (0.00–0.38 MPa; Table 2) are similar in magnitude to those estimated here (~0.0002 to ~0.564 MPa). In addition, in both the previous study and this study, the largest magnitude values of $\overline{\phi}(t_{eq}^{-})$ were estimated prior to the 1951 earthquake. However, in the previous study [*Lorenzo-Martín et al*., 2006], the geometry of the 1951 earthquake was modeled to overlap with the 1944 rupture, and as a result, total $\overline{\Delta CFS}(t_{eq}^{-})$ was negative (−2.92 to −3.30 MPa) although $\overline{\phi}(t_{eq}^{-})$ was positive.

Here we have used geodetically constrained two-layer models with Burgers rheologies, while previous three-dimensional viscoelastic studies of the 1939–1999 NAF [*Lorenzo-Martín et al*., 2006] have assumed layered Maxwell rheologies. Some differences in estimates of $\phi(t)$ between previous studies and this paper should be expected due to these different assumed rheologies. In addition, although the assumed effective coefficient of friction is the same ($\mu'=0.4$) in previous studies [*Lorenzo-Martín et al*., 2006] and the present study, both fault geometries and earthquake parameters differ. We use a simplified fault geometry in which all fault segments are connected in order to be consistent with a block model geometry [e.g., *Meade et al*., 2002; *Reilinger et al*., 2006; *DeVries et al*., 2014], while previous studies [*Lorenzo-Martín et al*., 2006] use fault geometries in which fault segments terminate. In addition, in the present study, we do not include the effects of the 1992, 1971, 1949, 1966 earthquakes; one previous (elastic) study takes into account all of these earthquakes but was published prior to the 1999 Izmit and Düzce earthquakes [*Stein et al*., 1997]. The previous viscoelastic study [*Lorenzo-Martín et al*., 2006] incorporates the effects of 1992 and the 1999 earthquakes, but not the 1971, 1966, and 1949 earthquakes.

In another recent study of stress transfer along the NAF [*Hearn et al*., 2002b], ΔCFS was estimated to increase by 15–25% due to the effects of time-dependent afterslip over 300 days after the 1999 earthquake in the Marmara Sea. Another study incorporating time-dependent afterslip over 87 days estimated a $\overline{\phi}$ value along the northern NAF in the Sea of Marmara of ~0.05 MPa [*Parsons*, 2004]. These estimates are based on frictional afterslip after the Izmit earthquake, and thus not directly analogous to the results reported here for layered viscoelastic models of the NAF earthquake sequence. However, in one of these previous studies [*Hearn et al*., 2002b], postseismic increases in ΔCFS due to viscoelastic effects of the 1999 earthquake were reported to be up to an order of magnitude greater than those due to frictional afterslip.

In a broader sense as well, the magnitudes of $\phi(t_{eq}^{-})$ along the NAF are comparable to estimates from earthquake sequences in the western United States and different tectonic settings around the world [*Freed and Lin*, 2001; *Zeng*, 2001; *Pollitz and Sacks*, 1995, 1997, 2002; *Pollitz et al*., 2003; *To et al*., 2004; *Freed and Lin*, 2002; *Casarotti and Piersanti*, 2003; *Nostro et al*., 2001].

In this discussion, we focus largely on the time-dependent quantity $\phi(t)$ as the evolution of this quantity may shed light on delayed earthquake triggering along the NAF and elsewhere. That said, we also note that there are significant differences between estimates of $\overline{\Delta CFS}(t_{eq}^{-})$ in this study and previous studies (Table 2, supporting information Table A1) [*Stein et al*., 1997; *Lorenzo-Martín et al*., 2006], although values $\phi\left(t_{eq}^{-}\right)$ are broadly similar (Table 2). In one previous study [*Lorenzo-Martín et al*., 2006], estimates of $\overline{\Delta CFS}(t_{eq}^{-})$ in the 1942, 1951, and 1967 earthquakes were negative (−0.67 to −0.48 MPa, −3.30 to −2.92 MPa, and −0.16 to −0.31 MPa respectively). However, in an earlier study of static ΔCFS, $\overline{\Delta CFS}_{elastic}(t_{eq}^{-})$ values for the 1942, 1951, and 1967 earthquakes were positive (0.13, 0.17, and 0.14 MPa respectively; (Supporting information Table A1) [*Stein et al*., 1997]. In the present study, we estimate positive values of $\overline{\Delta CFS}(t_{eq}^{-})$ for all earthquakes (supporting information Figure A4). In previous studies, $\overline{\Delta CFS}_{elastic}(t_{eq}^{-})$ for the 1943 earthquake has been estimated to be ~0 MPa [*Stein et al*., 1997] and ~0.04 MPa [*Lorenzo-Martín et al*., 2006]; here we estimate $\overline{\Delta CFS}_{elastic}(t_{eq}^{-})$ to be ~0.02 for this earthquake (supporting information Table A1).

A study of 29 $M_W > 6.0$ earthquakes in northwest Turkey and the Aegean Sea [*Nalbant et al*., 1998] concluded that the western Bay of Izmit was likely experiencing ΔCFS > 0.1 MPa prior to the 1999 Izmit earthquake.

Another study focused on seismic hazard in the Marmara Sea region [*Parsons et al.*, 2000] and estimated that the Izmit earthquake took place in a region of $\Delta CFS = 0.1–0.2$ MPa. In a subsequent study of static stress transfer due to earthquakes in the Sea of Marmara since 1700 [*King et al.*, 2001], $\Delta CFS^{\{h\}}_{elastic}(t^-_{eq})$ was estimated to be 0.05–0.20 MPa for the 1999 earthquake. The values of $\overline{\Delta CFS}(t^-_{eq})$ and $\Delta CFS^{\{h\}}(t^-_{eq})$ estimated here for the 1999 event (~0.165–0.200 and ~0.098–0.128 MPa respectively; Table 2) are comparable in magnitude. Finally, after the 1999 event, immediately to the west along the NAF in the Sea of Marmara, $\overline{\Delta CFS}_{elastic}$ has been estimated to be ~0.1–0.5 MPa [*King et al.*, 2001] and ~0.20 MPa [*Parsons*, 2004], consistent with the estimated $\overline{\Delta CFS}_{elastic}$ value of ~0.46 MPa estimated here.

Finally, the use of an effective coefficient of friction $\mu\prime$ in equation (1) assumes that pore pressure across a fault plane is linearly related to the confining stress [*Rice and Cleary*, 1976; *Roeloffs*, 1988; *Reasenberg and Simpson*, 1992]. This may well be a valid assumption immediately after an earthquake, but over longer timescales changes in pore fluid pressure may play a more complicated role in stress transfer and earthquake triggering [e.g., *Harris*, 1998; *King and Cocco*, 2001]. We have so far assumed a μ' of 0.4, but previous studies have suggested values of μ' as small as 0.0–0.2 [e.g., *Reasenberg and Simpson*, 1992; *Harris*, 1998; *King and Cocco*, 2001] and larger than 0.7 [e.g., *Stein et al.*, 1997]. The migration of fluids may lead to spatial and temporal variations in μ' [*Reasenberg and Simpson*, 1992; *Harris*, 1998] and effective coefficients of friction may also vary with faulting mechanism [e.g., *Parsons et al.*, 1999]. On the other hand, aftershock studies [*King et al.*, 1994] have also found that correlations between aftershock locations and Coulomb failure stress do not depend strongly on $\mu\prime$ [*King et al.*, 1994; *Freed*, 2005].

Although a detailed treatment of the role of pore pressure changes in stress transfer is beyond the scope of this paper, we calculated $\Delta CFS(t)$, and $\phi(t)$, along the NAF for a range of values of $\mu\prime$. Overall, variations in $\mu\prime$ result in relatively modest changes in the values of $\overline{\Delta CFS}(t^-_{eq})$, $\Delta CFS^{\{h\}}(t^-_{eq})$, $\overline{\phi}(t^-_{eq})$, and $\phi^{\{h\}}(t^-_{eq})$. This might be expected because of the relatively linear trace of the NAF system and patterns of CFS changes after strike slip earthquakes [e.g., *King et al.*, 1994]. Values of $\overline{\Delta CFS}(t^-_{eq})$ and $\overline{\phi}(t^-_{eq})$MPa changed by up to ~25% with variations in $\mu\prime$ from 0.2 to 0.8. However, these changes do not significantly affect the overall pattern of stress changes along the fault.

The results presented here have significant implications for not only the static Coulomb failure stress changes along the northern strand of the NAF in the Sea of Marmara, but also the time evolution of stress. By ~2023, $\overline{\phi}(t)$ along the 1766 earthquake rupture length may reach or exceed the apparent mean time-dependent stress thresholds $\overline{\phi}(t^-_{eq})$ for all seven previous 1939–1999 earthquakes. Together these results suggest that if the eastern NAF behaves similarly to the central and western NAF, the eastern NAF that previously ruptured in 1766 may be at high risk of rupturing again within the next decade.

6. Conclusions

Viscoelastic stress transfer models of the 1939–1999 earthquake sequence using geodetically constrained Burgers rheologies suggest that the mean viscoelastic component of Coulomb failure stress along each rupture length, $\overline{\phi}(t^-_{eq})$, is positive. In other words, viscoelastic stress diffusion between major earthquakes loads the hypocenters of next earthquakes in the sequence. Although the values of $\overline{\phi}(t^-_{eq})$ vary by two orders of magnitude, the mean across all seven earthquakes is between ~0.13 and ~0.21 MPa. The mean ΔCFS along the earthquake rupture extents may increase by up to ~177% due to noncoseismic viscoelastic effects. Finally, the stress transfer calculations suggest that by ~2023, $\overline{\phi}(t)$ along the easternmost strand of the NAF in the Marmara Sea may reach or exceed the values f $\overline{\phi}(t^-_{eq})$ for all seven previous 1939–1999 earthquakes. These time-dependent stress changes may be especially significant to consider from a seismic hazard perspective because the Marmara Sea strand of the NAF runs less than 50 km from Istanbul, a city of more than 14 million people.

Acknowledgments
We thank three anonymous reviewers and editor Thorsten Becker for thoughtful reviews that led to substantial improvements. All data referred to in the paper is properly cited and referred to in the reference list. The computations in this paper were run on the Odyssey cluster supported by the FAS Division of Science, Research Computing Group at Harvard University. This work was supported by the Harvard University and the Department of Energy Computational Science Graduate Fellowship Program of the Office of Science and National Nuclear Security Administration in the Department of Energy under contract DE-FG02-97ER25308.

References

Ambraseys, N. (2002), The seismic activity of the Marmara Sea region over the last 2000 years, *Bull. Seismol. Soc. Am.*, *92*(1), 1–18.
Ambraseys, N. N., and J. A. Jackson (2000), Seismicity of the Sea of Marmara (Turkey) since 1500, *Geophys. J. Int.*, *141*(3), F1–F6.
Anderson, J. G., J. N. Brune, J. N. Louie, Y. Zeng, M. Savage, G. Yu, and Q. Chen (1994), Seismicity in the western Great Basin apparently triggered by the Landers, California, earthquake, 28 June 1992, *Bull. Seismol. Soc. Am.*, *84*(3), 863–891.
Atkinson, B. K. (1984), Subcritical crack growth in geological materials, *J. Geophys. Res.*, *89*(B6), 4077–4114.
Barka, A. (1992), The North Anatolian fault zone, *Ann. Tect. Special Issue, Supplement to Volume IV*, 164–195.

Barka, A. (1996), Slip distribution along the North Anatolian fault associated with the large earthquakes of the period 1939 to 1967, *Bull. Seismol. Soc. Am.*, *86*(5), 1238–1254.
Barka, A. (1999), The 17 August 1999 Izmit Earthquake, *Science*, *285*, 1858–1859.
Bell, M. A., J. R. Elliott, and B. E. Parsons (2011), Interseismic strain accumulation across the Manyi (Tibet) prior to the 1997 MW 7.6 earthquake, *Geophys. Res. Lett.*, *38*, L24302, doi:10.1029/2011GL049762.
Brodsky, E. E., and S. G. Prejean (2005), New constraints on mechanisms of remotely triggered seismicity at Long Valley Caldera, *J. Geophys. Res.*, *110*, B04302, doi:10.1029/2004JB003211.
Brodsky, E. E., E. Roeloffs, D. Woodcock, I. Gall, and M. Manga (2003), A mechanism for sustained groundwater pressure changes induced by distant earthquakes, *J. Geophys. Res.*, *108*(B8), 2390, doi:10.1029/2002JB002321.
Bürgmann, R., S. Ergintav, P. Segall, E. Hearn, S. McClusky, R. E. Reilinger, H. Woith, and J. Zchau (2002), Time-dependent distributed afterslip on and deep below the Izmit Earthquake rupture, *Bull. Seismol. Soc. Am.*, *92*(1), 126–137.
Casarotti, E., and A. Piersanti (2003), Postseismic stress diffusion in Chile and South Peru, *Earth Planet. Sci. Lett.*, *206*(3), 325–333.
ChaoJun, Z., C. JianLing, and S. YaoLin (2009), Studying the viscosity of lower crust of Qinghai-Tibet Plateau according to post-seismic deformation, *Sci. China Ser. D*, *52*(3), 411–419.
de Hoog, F. R., J. H. Knight, and A. N. Stokes (1982), An improved method for numerical inversion of Laplace transforms, *SIAM J. Sci. Stat. Comput.*, *3*(3), 357–366.
Deng, J., and L. R. Sykes (1997a), Evolution of the stress field in southern California and triggering of moderate-size earthquakes: A 200-year perspective, *J. Geophys. Res.*, *102*, 9859–9886.
Deng, J., and L. R Sykes (1997b), Stress evolution in southern California and triggering of moderate-, small-, and micro-size earthquake, *J. Geophys. Res.*, *102*, 24,411–24,435.
DeVries, P. M. R., and B. J. Meade (2013), Earthquake cycle deformation in the Tibetan plateau with a weak mid-crustal layer, *J. Geophys. Res. Solid Earth*, *118*, 3101–3111, doi:10.1002/jgrb.50209.
DeVries, P. R., P. Krastev, and B. Meade (2014), *Toward viscoelastic block models of the North Anatolian fault: Integrating geodetic and delayed stress triggering constraints in three-dimensions, Abstract T34B-06*, AGU, San Francisco, Calif.
Dieterich, J. H. (1992), Earthquake nucleation on faults with rate-and state-dependent strength, *Tectonophysics*, *211*(1), 115–134.
Dieterich, J. H. (1994), A constitutive law for rate of earthquake production and its application to earthquake clustering, *J. Geophys. Res.*, *99*, 2601.
Doser, D. I., and R. Robinson (2002), Modeling stress changes induced by earthquakes in the southern Marlborough region, South Island, New Zealand, *Bull. Seismol. Soc. Am.*, *92*(8), 3229–3238.
Eberhart-Phillips, D., et al. (2003), The 2002 Denali fault earthquake, Alaska: A large magnitude, slip-partitioned event, *Science*, *300*(5622), 1113–1118.
Ergintav, S., et al. (2009), Seven years of postseismic deformation following the 1999, M=7.4 and M=7.2, Izmit-Düzce, Turkey earthquake sequence, *J. Geophys. Res.*, *114*, B07403, doi:10.1029/2008JB006021.
Freed, A. M. (2005), Earthquake triggering by static, dynamic, and postseismic stress transfer, *Ann. Rev. Earth Planet. Sci.*, *33*, 335–367.
Freed, A. M., and J. Lin (2001), Delayed triggering of the 1999 Hector Mine earthquake by viscoelastic stress transfer, *Nature*, *411*(6834), 180–183.
Freed, A. M., and J. Lin (2002), Accelerated stress buildup on the southern San Andreas fault and surrounding regions caused by Mojave Desert earthquakes, *Geology*, *30*(6), 571–574.
Fukahata, Y., and M. Matsu'ura (2005), General expressions for internal deformation fields due to a dislocation source in a multilayered elastic half-space, *Geophys. J. Int.*, *161*(2), 507–521.
Fukahata, Y., and M. Matsu'ura (2006), Quasi-static internal deformation due to a dislocation source in a multilayered elastic/viscoelastic half-space and an equivalent theorem, *Geophys. J. Int.*, *166*(1), 418–432.
Gomberg, J., P. A. Reasenberg, P. Bodin, and R. A. Harris (2001), Earthquake triggering by seismic waves following the Landers and Hector Mine earthquakes, *Nature*, *411*(6836), 462–466.
Gomberg, J., P. Bodin, K. Larson, and H. Dragert (2004), Earthquake nucleation by transient deformations caused by the M=7.9 Denali, Alaska, earthquake, *Nature*, *427*(6975), 621–624.
Gonzalez-Huizar, H., A. A. Velasco, Z. Peng, and R. R. Castro (2012), Remote triggered seismicity caused by the 2011 M9.0 Tohoku-Oki, Japan earthquake, *Geophys. Res. Lett.*, *39*, L10302, doi:10.1029/2012GL051015.
Hardebeck, J. L., J. J. Nazareth, and E. Hauksson (1998), The static stress change triggering model: Constraints from two southern California aftershock sequences, *J. Geophys. Res.*, *103*, 24,427–24,437.
Harris, R. A. (1998), Introduction to special section: Stress triggers, stress shadows, and implications, *J. Geophys. Res.*, *103*, 24,347–24,358.
Harris, R. A., and R. W. Simpson (1992), Changes in static stress on southern California faults after the 1992 Landers earthquake, *Nature*, *360*, 251–254.
Hashima, A., M. Fukahata, C. Hashimoto, and M. Matsu'ura (2014), Quasi-static strain and stress fields due to a moment tensor in elastic-viscoelastic layered half-space, *Pure Appl. Geophys.*, *171*(8), 1669–1693.
Hearn, E. H., and W. R. Thatcher (2015), Reconciling viscoelastic models of postseismic and interseismic deformation: Effects of viscous shear zones and finite-length ruptures, *J. Geophys. Res. Solid Earth*, *120*, 2794–2819, doi:10.1002/2014JB011361.
Hearn, E. H., B. H. Hager, and R. E. Reilinger (2002a), Viscoelastic deformation from North Anatolian fault zone earthquakes and the eastern Mediterranean GPS velocity field, *Geophys. Res. Lett.*, *29*(11), doi:10.1029/2002GL014889.
Hearn, E. H., R. Bürgmann, and R. E. Reilinger (2002b), Dynamics of Izmit earthquake postseismic deformation and loading of the Düzce earthquake hypocenter, *Bull. Seismol. Soc. Am.*, *92*(1), 172–193.
Hearn, E. H., S. McClusky, S. Ergintav, and R. E. Reilinger (2009), Izmit earthquake postseismic deformation and dynamics of the North Anatolian fault zone, *J. Geophys. Res.*, *114*, B08405, doi:10.1029/2008JB006026.
Hetland, E. (2006), Models of interseismic deformation with an analytic framework for the inclusion of general linear viscoelastic rheologies, PhD thesis, 255 p., Massachusetts Inst. of Technol., Boston, Mass.
Hetland, E. A., and B. H. Hager (2003), Postseismic relaxation across the central Nevada seismic belt, *J. Geophys. Res.*, *108*(B8), 2394, doi:10.1029/2002JB002257.
Hetland, E. A., and B. H. Hager (2006), The effects of rheological layering on post-seismic deformation, *Geophys. J. Int.*, *166*(1), 277–292.
Hill, D. P., et al. (1993), Seismicity remotely triggered by the magnitude 7.3 Landers, California, earthquake, *Science*, *260*(5114), 1617–1623.
Hollenbeck, K. J. (1998), INVLAP.M: A matlab function for numerical inversion of Laplace transforms by the de Hoog algorithm. [Available at http://www.isva.dtu.dk/staff/karl/invlap.htm.]

Jónsson, S., P. Segall, R. Pedersen, and G. Bjornsson (2003), Post-earthquake ground movements correlated to pore-pressure transients, *Lett. Nat.*, *424*, 179–183.
Kilb, D., J. Gomberg, and P. Bodin (2000), Triggering of earthquake aftershocks by dynamic stresses, *Nature*, *408*(6812), 570–574.
Kilb, D., J. Gomberg, and P. Bodin (2002), Aftershock triggering by complete Coulomb stress changes, *J. Geophys. Res.*, *107*(B4), doi:10.1029/2001JB000202.
King, G. C., R. S. Stein, and J. Lin (1994), Static stress changes and the triggering of earthquakes, *Bull. Seismol. Soc. Am.*, *84*(3), 935–953.
King, G. C. P., and M. Cocco (2001), Fault interaction by elastic stress changes: New clues from earthquake sequences, *Adv . Geophys.*, *44*, 1–38.
King, G. C., A. Hubert-Ferrari, S. S. Nalbant, B. Meyer, R. Armijo, and D. Bowman (2001), Coulomb interactions and the 17 August 1999 Izmit, Turkey earthquake, *C. R. Acad. Sci.*, *333*(9), 557–569.
Lorenzo-Martín, F., F. Roth, and R. Wang (2006), Elastic and inelastic triggering of earthquakes in the North Anatolian fault zone, *Tectonophysics*, *424*(3), 271–289.
Marsan, D., and C. J. Bean (2003), Seismicity response to stress perturbations, analysed for a world-wide catalogue, *Geophys. J. Int.*, *154*(1), 179–195.
Matsu'ura, M., and R. Sato (1975), Static deformation due to the fault spreading over several layers in a multi-layered medium Part II: Strain and tilt, *J. Phys. Earth*, *23*(1), 1–29.
Matsu'ura, M., and T. Sato (1989), A dislocation model for the earthquake cycle at convergent plate boundaries, *Geophys. J. Int.*, *96*(1), 23–32.
Meade, B. J., et al. (2002), Estimates of seismic potential in the Marmara Sea region from block models of secular deformation constrained by global positioning system measurements, *Bull. Seismol. Soc. Am.*, *92*(1), 208–215.
Meade, B. J., Y. Klinger, and E. A. Hetland (2013), Inference of multiple earthquake-cycle relaxation timescales from irregular geodetic sampling of interseismic deformation, *Bull. Seismol. Soc. Am.*, *103*(5), 2824–2835.
Nalbant, S. S., A. Hubert, and G. C. King (1998), Stress coupling between earthquakes in northwest Turkey and the north Aegean Sea, *J. Geophys. Res.*, *103*, 24,469–24,486.
Nostro, C., A. Piersanti, and M. Cocco (2001), Normal fault interaction caused by coseismic and postseismic stress changes, *J. Geophys. Res.*, *106*, 19,391–19,410.
Nur, A. and G. Mavko (1974), Postseismic Viscoelastic Rebound, *Science*, *183*(4121), 204–206.
Okada, Y. (1992), Internal deformation due to shear and tensile faults in a half-space, *Bull. Seismol. Soc. Am.*, *82*(2), 1018–1040.
Parsons, T. (2004), Recalculated probability of M≥7 earthquake beneath Sea of Marmara, Turkey, *J. Geophys. Res.*, *109*, B05304, doi:10.1029/2003JB002667.
Parsons, T., R. S. Stein, R. W. Simpson, and P. A. Reasenberg (1999), Stress sensitivity of fault seismicity: A comparison between limited-offset oblique and major strike-slip faults, *J. Geophys. Res.*, *104*, 20,183–20,202.
Parsons, T., S. Toda, R. S. Stein, A. Barka, and J. H. Dieterich (2000), Heightened odds of large earthquakes near Istanbul: An interaction-based probability calculation, *Science*, *288*(5466), 661–665.
Parsons, T., and D. S. Dreger (2000), Static-stress impact of the 1992 Landers earthquake sequence on nucleation and slip at the site of the 1999 M = 7.1 Hector Mine earthquake, southern California, *Geophys. Res. Lett.*, *27*(13), 1949–1952.
Pollitz, F. F., and I. S. Sacks (1995), Consequences of stress changes following the 1891 Nobi earthquake, Japan, *Bull. Seismol. Soc. Am.*, *85*(3), 796–807.
Pollitz, F. F., and I. S. Sacks (1997), The 1995 Kobe, Japan, earthquake: A long-delayed aftershock of the offshore 1944 Tonankai and 1946 Nankaido earthquakes, *Bull. Seismol. Soc. Am.*, *87*(1), 1–10.
Pollitz, F. F., and I. S. Sacks (2002), Stress triggering of the 1999 Hector Mine earthquake by transient deformation following the 1992 Landers earthquake, *Bull. Seismol. Soc. Am.*, *92*(4), 1487–1496.
Pollitz, F. F., R. Bürgmann, and B. Romanowicz (1998), Viscosity of oceanic asthenosphere inferred from remote triggering of earthquakes, *Science*, *280*(5367), 1245–1249.
Pollitz, F., M. Vergnolle, and E. Calais (2003), Fault interaction and stress triggering of twentieth century earthquakes in Mongolia, *J. Geophys. Res.*, *108*(B10), 2503, doi:10.1029/2002JB002375.
Pollitz, F. F., R. S. Stein, V. Sevilgen, and R. Bürgmann (2012), The 11 April 2012 East Indian Ocean earthquake triggered large aftershocks worldwide, *Nature*, *490*(7419), 250–253.
Prejean, S. G., et al. (2004), Remotely triggered seismicity on the United States west coast following the Mw 7.9 Denali fault earthquake, *Bull. Seismol. Soc. Am.*, *94*(6B), S348–S359.
Reasenberg, P. A., and R. W. Simpson (1992), Response of regional seismicity to the static stress change produced by the Loma Prieta earthquake, *Science*, *255*(5052), 1687–1690.
Reilinger, R., and S. McClusky (2001), GPS constraints on block motions and deformations in western Turkey and the Aegean: Implications for earthquake hazards, in Seismotectonics of the Northwestern Anatolia-Aegean and Recent Turkish Earthquakes, pp. 14–20, edited by T. Taymaz, *Istanbul Tech. Univ.*, Istanbul, Turkey.
Reilinger, R., et al. (2006), GPS constraints on continental deformation in the Africa-Arabia-Eurasia continental collision zone and implications for the dynamics of plate interactions, *J. Geophys. Res.*, *111*, B05411, doi:10.1029/2005JB004051.
Rice, J. R., and M. P. Cleary (1976), Some basic stress diffusion solutions for fluid-saturated elastic porous media with compressible constituents, *Rev. Geophys.*, *14*(2), 227–241.
Roeloffs, E. A. (1988), Fault stability changes induced beneath a reservoir with cyclic variations in water level, *J. Geophys. Res.*, *93*, 2107–2124.
Roth, F. (1988), Modelling of stress patterns along the western part of the North Anatolian fault zone, *Tectonophysics*, *152*(3), 215–226.
Ryder, I., R. Bürgmann, and F. Pollitz (2011), Lower crustal relaxation beneath the Tibetan Plateau and Qaidam Basin following the 2001 Kokoxili earthquake, *Geophys. J. Int.*, *187*(2), 613–630.
Ryder, I., B. Parsons, T. J. Wright, and G. J. Funning (2007), Post-seismic motion following the 1997 Manyi (Tibet) earthquake: InSAR observations and modeling, *Geophys. J. Int.*, *169*(3), 1009–1027.
Sato, R. (1971), Crustal deformation due to dislocation in a multi-layered medium, *J. Phys. Earth*, *19*(1), 31–46.
Sato, R., and M. Matsu'ura (1973), Static deformation due to the fault spreading over several layers in a multi-layered medium. Part I: Displacement, *J. Phys. Earth*, *21*, 227–249.
Sato, T., and Matsu'ura (1988), A kinematic model for deformation of the lithosphere at subduction zones, *J. Geophys. Res.*, *93*, 6410–6418.
Savage, J. C., and W. H. Prescott (1978), Asthenosphere readjustment and the earthquake cycle, *J. Geophys. Res.*, *83*, 3369–3376.

Steacy, S., J. Gomberg, and M. Cocco (2005), Introduction to special section: Stress transfer, earthquake triggering, and time-dependent seismic hazard, *J. Geophys. Res.*, *110*, B05S01, doi:10.1029/2005JB003692.

Stein, R. S. (2003), Earthquake conversations, *Sci. Am.*, *288*(1), 72–79.

Stein, R. S., A. A. Barka, and J. H. Dieterich (1997), Progressive failure on the North Anatolian fault since 1939 by earthquake stress triggering, *Geophys. J. Int.*, *128*(3), 594–604.

To, A., R. Bürgmann, and F. Pollitz (2004), Postseismic deformation and stress changes following the 1819 Rann of Kachchh, India earthquake: Was the 2001 Bhuj earthquake a triggered event? *Geophys. Res. Lett.*, *31*, L13609, doi:10.1029/2004GL020220.

Tselentis, G. A., and J. Drakopoulos (1990), Stress transfer and nonlinear stress accumulation at the North Anatolian fault, Turkey, *Pure Appl. Geophys.*, *132*(4), 699–710.

Verdecchia, A., and S. Carena (2015), One hundred and fifty years of Coulomb stress history along the California-Nevada border, USA, *Tectonics*, *34*(2), 213–231.

Yamasaki, T., T. J. Wright, and G. A. Houseman (2014), Weak ductile shear zone beneath a major strike-slip fault: Inferences from earthquake cycle model constrained by geodetic observations of the western North Anatolian fault zone, *J. Geophys. Res. Solid Earth*, *119*, 3678–3699, doi:10.1002/2013JB010347.

Zeng, Y. (2001), Viscoelastic stress-triggering of the 1999 Hector Mine Earthquake by the 1992 Landers Earthquake, *Geophys. Res. Lett.*, *28*(15), 3007–3010.

Zhang, P., et al. (2004), Continuous deformation of the Tibetan Plateau from global positioning system data, *Geology*, *32*(9), 809–812.